Electric Field Alignment of a Block Copolymer Nanopattern: Direct Observation of the Microscopic Mechanism

Violetta Olszowka,[†] Markus Hund,[†] Volker Kuntermann,[‡] Sabine Scherdel,[§] Larisa Tsarkova,[†] and Alexander Böker[†,⊥,*]

[†]Lehrstuhl für Physikalische Chemie II, Universität Bayreuth, D-95440 Bayreuth, Germany, [‡]Lehrstuhl für Theoretische and Physikalische Chemie, Universität Erlangen, D-91058 Erlangen, Germany, and [§]Lehrstuhl für Chemische Physik, TU Chemnitz, D-09107 Chemnitz, Germany. [⊥]Present address: Lehrstuhl für Makromolekulare Materialien and Oberflächen and DWI an der RWTH Aachen e.V., RWTH Aachen University, 52056 Aachen, Germany.

ABSTRACT Using quasi-*in-situ* scanning force microscopy we study the details of nanopattern alignment in ABC terblock copolymer thin films in the presence of an in-plane electric field. Because of the surface interactions and electric field the lamellae are oriented both perpendicular to the plane of the film and parallel to the electric field. We identified two distinct defect types which govern the orientation mechanism. Ring-like (tori) and open-end defects dominate at the early stage of the orientation process, while mainly classic topological defects (disclinations and dislocations) are involved in long-range ordering at the late stages. Comparison of the time evolution of the defect density with the evolution of the orientational order parameter suggests that tori-defects are essential for the effective reorientation. Further, the quasi-*in-situ* SFM imaging allowed us to elucidate the influence of the electric field strength on the propagation velocity of the topological defects.

KEYWORDS: *in situ* scanning force microscopy · block copolymer · topological defects · nanopattern orientation · electric field · alignment mechanism

The spontaneous formation of nanostructured materials *via* molecular self-assembly of block copolymers attracts increasing scientific interest which is dictated by a growing number of technological applications of nanopatterns.[1] A serious challenge is to achieve a macroscopically long-range orientation and order or even a single-grain structure. Various procedures leading to high degrees of order have been successfully implemented both in bulk phases,[2−9] and in thin block copolymer films. Most of them utilize external fields such as electrical [6,10−14] or mechanical fields,[2,4,5,15−17] temperature gradients[9] or grapho-epitaxy.[18−20]

The key to an understanding of the orientation behavior of block copolymer microdomains in thin films is the knowledge of the underlying microscopic mechanisms which contribute to the rearrangement of domains. While shear and electric field alignment of block copolymers in bulk have been studied by a variety of different techniques such as *in situ* birefringence,[3] *in situ* small angle neutron scattering,[21] "*ex situ*" [5,22,23] and *in situ* small-angle scattering (SAXS),[24−26] little is known about the relevant processes of block copolymer alignment under electric fields in thin films. So far, experimental studies on the phase behavior in block copolymer films subjected to electric fields did not reveal information on the dynamics of single lamellae domains or on the dynamics of defects.

The use of electric fields for the alignment of lamellar microdomains in thin films has been demonstrated recently.[13,27,28] Because of the difference in the dielectric constants of the blocks (here: $\varepsilon_{PS} \approx 2.4$, $\varepsilon_{PMMA} \approx 3.6$),[29] the microdomains tend to orient parallel to the electric field vector thereby lowering the free energy of the system. Thus, striped patterns with long-range order were created *via* the combination of an electric field oriented within the plane of the film and of surface interactions tailored to favor a perpendicular orientation of the lamellae as has been described previously.[13,27,28]

In the present work we followed the structural evolution of the alignment in electric field *via* quasi-*in-situ* scanning force microscopy (SFM) using a newly developed SFM setup which allows solvent vapor treatment in the presence of electric fields (Figure 1). Quasi-*in-situ* SFM imaging, first demonstrated by successive plasma etching of thin polymer films[30] provides the possibility to reposition the SFM probe on a specific sample spot after *ex situ* treatment with

*Address correspondence to boeker@dwi.rwth-aachen.de.

Received for review January 28, 2009 and accepted April 03, 2009.

Published online April 22, 2009.
10.1021/nn900081u CCC: $40.75

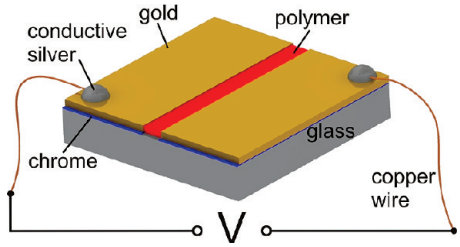

Figure 1. Schematic of electrodes on a glass substrate. The thickness of the chrome and gold layer (5 nm + 50 nm) and the gap between the electrodes (10 μm) are not true to scale. The size of the arrangement (sample size) is about 6 mm × 6 mm × 1 mm. The electric field is homogeneous between the electrodes. Details can be found in the Supporting Information.

high accuracy with respect to the lateral displacement between tip and sample. This technique allows the straightforward examination of the same sample spot prior to and after sample treatment. Using the above approach we compared the density of two particular defect types with the evolution of the orientational order parameter during the alignment process revealing the essential role of tori-defects for the lamella-reorientation mechanism. Further, the quasi-*in-situ* technique allowed us to elucidate the influence of the electric field strength on the propagation velocity of the topological defects.

RESULTS AND DISCUSSION

Microdomain Alignment in the Electric Field. Figure 2a displays a SFM phase image of a spin-coated $S_{47}H_{10}M_{43}^{82}$ film which has a disordered surface structure. The ordering effect of the simultaneous solvent vapor annealing and application of a voltage between the electrodes is shown in Figure 2b. After 6.5 h of treatment the stripe pattern appears highly ordered parallel to the electric field vector. Importantly, during the swelling of the film the polar middle PHEMA block remains anchored to the substrate which preserves the self-assembled stripe pattern of the two majority PS and PMMA blocks (Figure 2c).

Quasi *in Situ* Imaging. To elucidate the mechanism of microdomain alignment we used the newly developed quasi-*in-situ* SFM. Due to the high electric field strength and the sharp SFM tip it is impossible to perform *in situ* scanning in the presence of the electric field. The electric field would produce SFM artifacts caused by additional electrostatic forces between tip and sample. Moreover the applied voltage can easily damage the piezoelectric scanner by flashovers. Performing *ex situ* sample treatments with the aim to image the same spot on the sample prior to and after annealing would require time-consuming repositioning protocols. Moreover, this may not at all be feasible because of rather abrupt changes in the structure during the snapshot treatment in the electric field.[31] With the experimental setup used here we overcome the described above problems.[13]

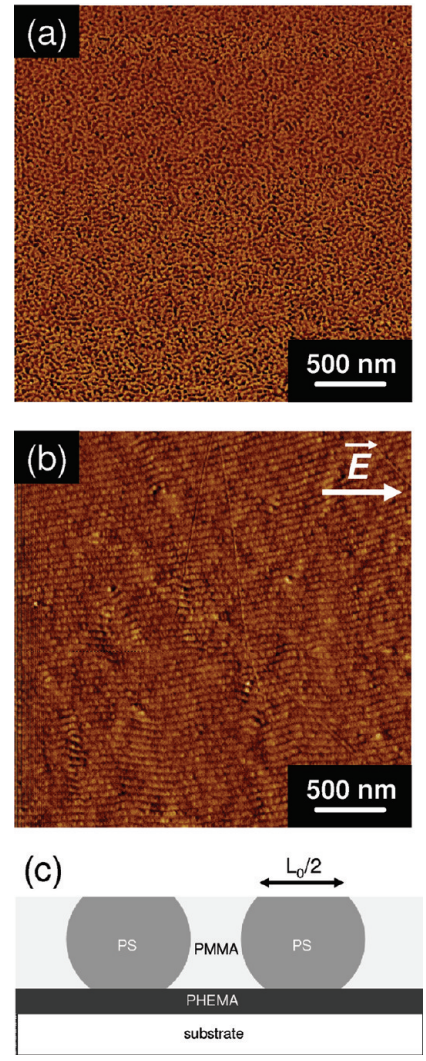

Figure 2. SFM phase ($\Delta\varphi = 0-20°$) images of a 39 nm thick $S_{47}H_{10}M_{43}^{82}$ film (a) after spin coating and (b) after annealing for 6.5 h in saturated toluene vapor at 15 V/μm. (c) Schematics of the microphase separated structure in an ultrathin ABC block copolymer film with the short middle block selectively anchored to the substrate. Reprinted from ref 44. Copyright 2001, American Chemical Society.

Further our approach is validated by comparison of the treatment time when the sample is treated continuously and when it is treated stepwise for snapshot imaging. Since in both cases the complete orientation of the stripe pattern along the electric field vector is achieved within 6−7 h, we concluded that the quasi-*in-situ* treatment has no significant effect on the mechanism of the microdomain alignment and ordering.

In Figure 3, the evolution of the initially disordered structure (Figure 3a) into an aligned lamellar array (Figure 3i) is shown as a function of the treatment time. Fifteen SFM images have been recorded during the orientation process at the same sample spot and were compiled into a movie (available in the Supporting Information). Nine images are exemplified in Figure 3.

In the following, the most representative defects at different time-scales of the structure evolution are identified and quantitatively analyzed. Ringlike defects (tori-

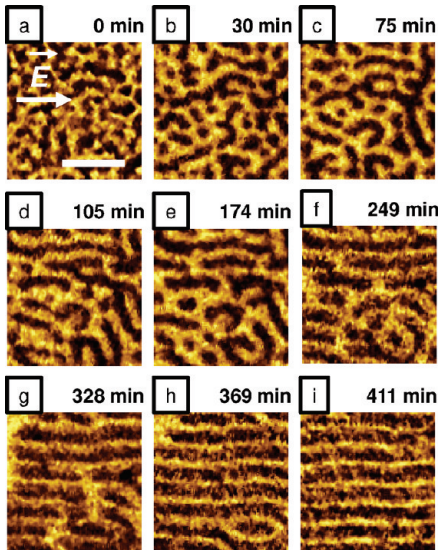

Figure 3. Crops (150 nm × 150 nm) from registered SFM phase images (snapshots taken from the SFM movie, which is available in the Supporting Information) illustrating the transition from the disordered structure (a) to highly ordered striped pattern (i). The film was annealed in saturated chloroform vapor under an electric field of 15 V/μm in the quasi-*in-situ* SFM chamber. The PMMA phase appears brighter in the images than the PS phase. The raw data were acquired by scanning areas of 3 × 3 μm² with 1024 × 1024 pixels using TappingMode imaging.

defects), as well as defect configurations with interrupted continuity of a lamella domain (open-end defects) dominate at the early stage of the orientation process, while only classical topological defects (disclinations and dislocations) are observed at the late stages of the long-range ordering, in agreement with recent observations.[32] In the SFM phase images the tori are represented by the harder PMMA-phase, which thus appears brighter than the PS-phase.

The snapshot imaging of the same spot revealed that the lamella alignment proceeds *via* creation, opening, and joining of tori-structures (Figure 3a−i). When the initially disordered pattern in Figure 3a is subjected to a 30-min-long treatment, the tori defects become clearly visible (Figure 3b). Within the next treatment steps the tori break/open (Figure 3c−f), and finally merge into straight lamellae (Figure 3g−i). On the one hand, merged tori form lamellae with the orientation parallel to the electric field vector, while on the other hand the merging of tori connects neighboring lamellae which are already oriented along the electric field *via* bridges (necks) (see, for example, Figure 3g). Such bridges allow the chain transport in the direction orthogonal to the PS-PMMA interface without crossing it. This kind of point defect was observed in the lyotropic lamellar liquid crystal phase,[33,34] and very recently in cylinder-forming block copolymer films with sufficient chain mobility.[32] Upon further annealing the bridges between ordered lamella annihilate (Figure 3h).

At the late stage of lamella orientation, classical topological defects (dislocations and disclinations) dominate[35,36] (Figures 3h and 4), and their movement

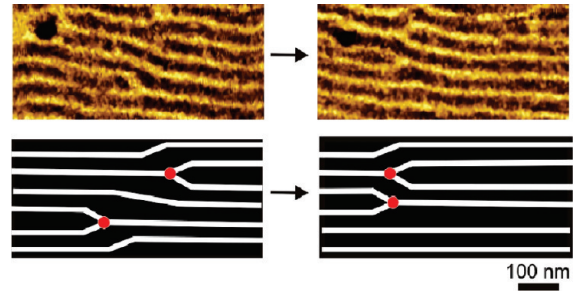

Figure 4. Details from quasi-*in-situ* SFM images showing the interaction of a (−)-dislocation and (+)-dislocation of PMMA under an electric field of 15 V/μm. The sketch below illustrates the movement of the defects. The propagation velocity amounts to $v = 192 \pm 5$ nm/h.

and annihilation can be followed in Figures 3h,i and 4. Figure 4 presents an example of the apparent topological defect interactions and their transformations. Displayed are two dislocations of PMMA which have an attractive interaction due to their opposite core sign. Therefore, in the next annealing step the dislocation is shifted one lamella up. This movement of defects toward each other is very similar to the process described recently by cell dynamics simulations.[37] The fact that the defects upon the applied snapshot treatment behave and interact in agreement with what is known about typical defects in block copolymers and in other kinds of soft and solid matter[38,39] is an additional confirmation that the stepwise annealing does not affect the ordering mechanism.

Evaluation of the Order Parameter. Important quantitative information regarding the alignment process was gained through a detailed analysis of the defect density and of the structure order parameter. Figure 5 shows the defect density of tori and of the open end defects as a function of time. The data was collected from 3 × 3 μm² SFM images. After short-term annealing of ~5 min, a similar density of tori and of open end defects (ca. 60 defects/μm²) was measured. Upon further treatment the number of open-end defects decreases exponentially until they vanish after ~370 min of the film treatment. In contrast, new tori defects are formed upon further annealing with

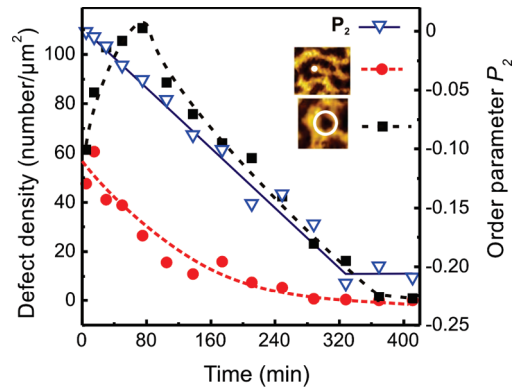

Figure 5. Time evolution of the defect density (left-hand axis) and of the orientational order parameter P_2 (right-hand axis) during the combined treatment under an electric field and solvent annealing. The lines are drawn as guides to the eye. The data was collected from 3 × 3 μm² SFM images.

the density reaching its maximum value of ca. 110 defects/μm^2 after ca. 80 min of the film treatment. Upon further annealing and corresponding ordering, the number of tori constantly decreases, and after ~410 min all tori are annihilated.

The order parameter as a function of time (Figure 5) shows an almost linear dependence and reaches a constant value of $P_2 = -0.21$ after approximately 320 min of the film treatment. Comparison of the time-evolution of the defect density (tori, open end defects) with the evolution of the order parameter P_2, suggests that open end defects are quickly annihilated during the alignment process, whereas tori-defects are generated to support the orientation process during its early stage. We note that open-end defects are generated as a result of the fast freezing of the structure during sample preparation by spin-coating, and they are energetically highly unfavorable due to the high local curvature of the interface. As a consequence, in the course of annealing their density is always smaller compared to the density of the tori.

The creation of the tori has the advantage that the polymer chains are able to diffuse along the A−B–C interface. If an electric field is applied, breaking of the tori along the electric field vector is favorable. To form a perfectly aligned structure, no translational movement of the center of mass of the tori is required. Simply breaking and merging the tori is sufficient. Thus such a ringlike structure is an ideal transition state during the reorientation process. Interestingly, similar ringlike defects were previously found in dynamic density functional theory simulations and TEM images of bulk SHM samples oriented from a concentrated solution under an electric field.[40,41] In addition, the creation of tori was also described in the smectic phase of liquid crystals[42] and in the cylinder phase of block copolymers[32,43] as a transient excited state.

Propagation of Topological Defects. Finally, we analyze the velocities of the topological defects during annealing at zero electric field and in the presence of an electric field. Figure 6a,b shows two examples for the propagation of dislocations after annealing in chloroform vapor at zero electric field and subsequent quench with argon. The defect velocities v were calculated *via* the changes in the *xy*-positions of the white points (marked in the images), and amount to 15 ± 5 nm/h. We note that the displayed dislocations are not surrounded by other defects and therefore any interaction forces can be excluded. When similar isolated defects are subjected to an electric field with a strength of $E = 15$ V/μm (Figure 6c,d), a distinct increase in defect velocity is detected. The dislocations in Figure 6c,d propagate at a velocity of $v = 93 \pm 5$ nm/h. In addition, we evaluated the propagation velocity of two dislocations with an opposite sign under an applied electric field of $E = 15$ V/μm (Figure 4). The two defects are found to independently approach one another with an average relative velocity of $v = 192 \pm 5$ nm/h, which is the sum of the absolute velocities of each individual dislocation and matches twice the velocity of an isolated defect. Thus, we can also exclude attractive interactions for this case.

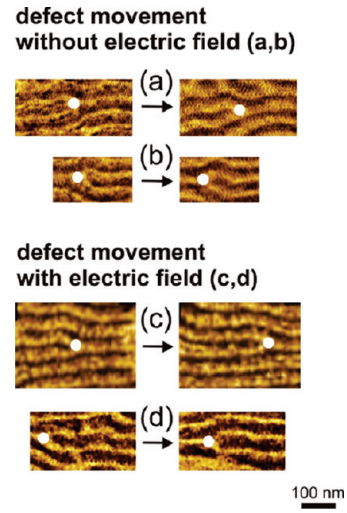

Figure 6. Propagation of classical defects at zero electric field (a,b), and at an electric field strength of $E = 15$ V/μm (c,d). The velocities were calculated *via* the change in the *xy*-positions of the white points, as marked in the images, and amount to $v = 15 \pm 5$ nm/h (a,b) and 93 ± 5 nm/h (c,d).

Using our quasi-*in-situ* SFM technique we were able to quantitatively evaluate the effect of an electric field on the propagation velocity of defects. The results revealed an increase of the defect velocity of almost an order of magnitude in the direction of the applied electric field.

CONCLUSION

In summary, we have shown that quasi-*in-situ* SFM measurements provide an important and detailed insight into the mechanism of microdomain alignment in thin block copolymer films. The time-resolved quasi-*in-situ* imaging yielded convincing evidence that in the studied system the orientation of the disordered phase under combined application of an electric field and solvent annealing proceeds through two major steps. First, in a rather rapid step, two dominant types of characteristic defects developed, which were described as tori and open-end defects. The latter defects are energetically less favorable and annihilate rapidly. The improvement of the structure orientation parallel to the electric field lines proceeds *via* rupture and rejoining of the tori-defects. The number density of tori defects shows a maximum at the early stage of the alignment process and finally decreased as a function of time, while the amount of open-end defects decreased steadily during the course of the treatment. At the later stage of alignment, a highly oriented structure was achieved *via* the movement and annihilation of the classical topological defects (dislocations and disclinations). Furthermore, the influence of the electric field on the velocity of isolated dislocations has been studied. It was shown, that under an electric field the defect velocity increases by about an order of magnitude in comparison to the defect velocity at zero electric field.

Finally, the quasi-*in-situ* SFM imaging has been proven to be a powerful tool for the investigation of complex orientation processes even under difficult experimental conditions. It allows the direct time-resolved visualization of the structure development on a nanoscopic scale.

METHODS

Polymer. A polystyrene-*b*-poly(2-hydroxyethyl methacrylate)-*b*-poly(methyl methacrylate) triblock copolymer was synthesized by sequential living anionic polymerization as described in detail elsewhere.[44] The polymer used in this study consists of 47 wt % polystyrene (PS), 10 wt % poly(2-hydroxyethyl methacrylate) (PHEMA) and 43 wt % poly(methyl methacrylate) (PMMA) with a total number−average molecular weight M_n = 82000 g/mol (we denote this material as $S_{47}H_{10}M_{43}^{82}$). Gel permeation chromatography of the final block copolymer yields a polydispersity of M_w/M_n = 1.04. Small angle X-ray scattering experiments on bulk samples (not shown here) indicate a lamellar morphology with characteristic lamellar spacing L_0 = 49 ± 6 nm. Films with a thickness of about 37 ± 2 nm (below L_0) were spin-cast from a 0.5 wt % toluene solution onto glass substrates and annealed in saturated chloroform vapor during the quasi-*in-situ* experiments at room temperature. In thin films a short PHEMA block acts as an anchor to the substrate. Therefore, the copolymer spontaneously forms an ultrathin brush layer terminated with the PS and PMMA blocks, on which the lamella structure resides, leading to a perpendicular orientation of the lamellae with respect to the substrate.

Electrodes. For the alignment experiments gold electrodes were evaporated onto a glass substrate. The electrode distance was chosen to 10 μm. The height of the electrodes was around 55 nm to compensate the swelling of the film in the presence of solvent vapor. A schematic of the electrode geometry is shown in Figure 1. Details on the distribution of the electric field lines and the field strength between the electrodes are shown in the Supporting Information.

Quasi-*in-Situ* SFM. The quasi-*in-situ* SFM setup utilizes a modified commercial SFM (Dimension 3100 equipped with a NanoScope IV SPM controller and a *XY* closed-loop scanner, all from Veeco Instruments, Inc.). A detailed description of the setup is reported elsewhere.[13,30,45] Si_3N_4 cantilevers from Olympus were used (OMCL-AC160TS, spring constant ~40 N/m, resonance frequency ranging from 200 to 300 kHz). All measurements were performed at free amplitudes of about 30−50 nm and a relative set point of about 0.95.

The sample treatment is executed as follows: The sample is located inside the chamber. The SFM scanner is retracted by some 8 mm from the sample. Then the chamber is closed by the lid. To anneal the sample successfully we perform the treatment in a hermetically sealed reactor chamber. The sample is exposed to chloroform vapor, while a voltage is applied across the electrodes on the glass substrate. The gas flow rate through the system was controlled by mass flow controllers and additionally checked by a flow meter installed at the outlet of the chamber. After a certain annealing time the solvent is removed with a flow of pure argon while the voltage is still applied in order to quench the structure in the presence of the electric field. Subsequently the lid is opened, the voltage is switched off, and the SFM scanner is approached to the sample. This procedure was repeated several times. The accomplishable position stability as a key performance feature of the quasi-*in-situ* SFM amounts to almost the same value as reported in ref 30 (low pressure plasma treatments). The increase in lateral drift is only about 23 nm per process step. The technical details will be published elsewhere. Thereby the SFM tip can easily and reliably be repositioned on a specific sample spot. The scan area (3 μm × 3 μm) was kept constant during the experiment. In a first postprocessing step the remaining lateral offsets between successive SFM images were corrected by maximization of the cross correlation between the images. To reduce nonlinear image distortions the images were then subsequently registered following the method described in ref 46. After registration a smaller detail of each SFM image was cut out to provide a series of images taken at exactly the same spot of the sample (see Figure 3 as an example).

Annealing Conditions. To estimate suitable annealing times, we followed the kinetics of swelling of the block copolymer films in the presence of chloroform vapor by spectroscopic ellipsometry as described elsewhere.[13] The equilibrium degree of swelling at a given vapor pressure is reached within a few minutes. A similar time span is found for the quenching of the film with argon to the final dry film thickness. Annealing times of several hours in saturated chloroform vapor (1.0 p_{sat} with a flow of 56 cm^3/min) under application of the electric field were chosen to ensure a high degree of microdomain ordering and alignment (Figure 2).

Orientational Order Parameter. To quantify the degree of microdomain alignment an order parameter P_2 was calculated according to

$$P_2 = \frac{3\langle\cos^2\varphi\rangle - 1}{2} \quad (1)$$

with

$$\langle\cos^2\varphi\rangle = \frac{\int_0^{2\pi} d\varphi\, (I_q(\varphi)\cos^2(\varphi)\,|\sin(\varphi)|)}{\int_0^{2\pi} d\varphi\, (I_q(\varphi)\,|\sin(\varphi)|)} \quad (2)$$

The angle φ quantifies the in plane direction with φ = 0° corresponding to the direction along the stripe-like electrodes. For an alignment of the lamellae along the field direction (maximum of azimuthal intensity distribution of the 2D Fourier-transform intensity at φ = 90°), P_2 ranges from 0 to −0.5 with P_2 = −0.5 corresponding to the fully oriented case.

Acknowledgment. This work was carried out in the framework of the Sonderforschungsbereich 481 (TP A2, B7, Z2) funded by the Deutsche Forschungsgemeinschaft (DFG). A. Böker acknowledges support by the Lichtenberg-Programm of the VolkswagenStiftung.

Supporting Information Available: Finite elements simulation of electric field strength and corresponding field lines between electrodes and SFM-movie showing the lamellae alignment in electric field. This material is available free of charge *via* the Internet at http://pubs.acs.org.

REFERENCES AND NOTES

1. Park, C.; Yoon, J.; Thomas, E. L. Enabling Nanotechnology with Self Assembled Block Copolymer Patterns. *Polymer* **2003**, *44*, 6725–6760.
2. Keller, A.; Pedemonte, E.; Willmouth, F. M. Macro-Lattice from Segregated Amorphous Phases of a 3 Block Copolymer. *Nature (London)* **1970**, *225*, 538–539.
3. Chen, Z. R.; Kornfield, J. A.; Smith, S. D.; Grothaus, J. T.; Satkowski, M. M. Pathways to Macroscale Order in Nanostructured Block Copolymers. *Science* **1997**, *277*, 1248–1253.
4. Albalak, R. J.; Thomas, E. L. Microphase Separation of Block Copolymer Solutions in a Flow Field. *J. Polym. Sci. Pol. Phys.* **1993**, *31*, 37–46.
5. Wiesner, U. Lamellar Diblock Copolymers under Large Amplitude Oscillatory Shear Flow: Order and Dynamics. *Macromol. Chem. Phys.* **1997**, *198*, 3319–3352.
6. Amundson, K.; Helfand, E.; Davis, D. D.; Quan, X.; Patel, S. S.; Smith, S. D. Effect of an Electric Field on Block Copolymer Microstructure. *Macromolecules* **1991**, *24*, 6546–6548.
7. Amundson, K.; Helfand, E.; Quan, X.; Smith, S. D. Alignment of Lamellar Block Copolymer Microstructure in an Electric Field. 1. Alignment Kinetics. *Macromolecules* **1993**, *26*, 2698–2703.

8. Amundson, K.; Helfand, E.; Quan, X.; Hudson, S. D.; Smith, S. D. Alignment of Lamellar Block Copolymer Microstructure in an Electric Field. 2. Mechanisms of Alignment. *Macromolecules* **1994**, *27*, 6559–6570.
9. Hashimoto, T.; Bodycomb, J.; Funaki, Y.; Kimishima, K. The Effect of Temperature Gradient on the Microdomain Orientation of Diblock Copolymers Undergoing an Order-Disorder Transition. *Macromolecules* **1999**, *32*, 952–954.
10. Morkved, T. L.; Lu, M.; Urbas, A. M.; Ehrichs, E. E.; Jaeger, H. M.; Mansky, P.; Russell, T. P. Local Control of Microdomain Orientation in Diblock Copolymer Thin Films with Electric Fields. *Science* **1996**, *273*, 931–933.
11. Thurn-Albrecht, T.; Schotter, J.; Kastle, G.A.; Emley, N.; Shibauchi, T.; Krusin-Elbaum, L.; Guarini, K.; Black, C.T.; Tuominen, M.T.; Russell, T.P. Ultrahigh-Density Nanowire Arrays Grown in Self-Assembled Diblock Copolymer Templates. *Science* **2000**, *290*, 2126–2129.
12. Böker, A.; Knoll, A.; Elbs, H.; Abetz, V.; Müller, A. H. E.; Krausch, G. Large Scale Domain Alignment of a Block Copolymer from Solution Using Electric Fields. *Macromolecules* **2002**, *35*, 1319–1325.
13. Olszowka, V.; Hund, M.; Kuntermann, V.; Scherdel, S.; Tsarkova, L.; Böker, A.; Krausch, G. Large Scale Alignment of a Lamellar Block Copolymer Thin Film *via* Electric Fields: A Time-Resolved SFM Study. *Soft Matter* **2006**, *2*, 1089–1094.
14. Xu, T.; Wang, J.; Russell, T. P. In *Nanostructured Soft Matter: Experiment, Theory, Simulation and Perspectives*; Zvelindovsky, A. V., Ed.; Springer, New York, 2007; pp 171−198.
15. Cheng, J. Y.; Ross, C. A.; Smith, H. I.; Thomas, E. L. Templated Self-Assembly of Block Copolymers: Top-Down Helps Bottom-Up. *Adv. Mater.* **2006**, *18*, 2505–2521.
16. Chen, Z.-R.; Kornfield, J. A. Flow-Induced Alignment of Lamellar Block Copolymer Melts. *Polymer* **1998**, *39*, 4679–4699.
17. Angelescu, D. E.; Waller, J. H.; Register, R. A.; Chaikin, P. M. Shear-Induced Alignment in Thin Films of Spherical Nanodomains. *Adv. Mater.* **2005**, *17*, 1878–1881.
18. Segalman, R. A.; Yokoyama, H.; Kramer, E. J. Graphoepitaxy of Spherical Domain Block Copolymer Films. *Adv. Mater.* **2001**, *13*, 1152–1155.
19. Kim, S. H.; Misner, M. J.; Xu, T.; Kimura, M.; Russell, T. P. Highly Oriented and Ordered Arrays from Block Copolymers *via* Solvent Evaporation. *Adv. Mater.* **2004**, *16*, 226–231.
20. Yoon, J.; Lee, W.; Thomas, E. L. Highly Oriented Thin-Film Microdomain Patterns of Ultrahigh Molecular Weight Block Copolymers *via* Directional Solidification of a Solvent. *Adv. Mater.* **2006**, *18*, 2691–2694.
21. Balsara, N. P.; Hammouda, B. Shear Effects on Solvated Block-Copolymer Lamellae−Polystyrene−Polyisoprene in Dioctyl Phthalate. *Phys. Rev. Lett.* **1994**, *72*, 360–363.
22. Winey, K. I.; Patel, S. S.; Larson, R. G.; Watanabe, H. Morphology of a Lamellar Diblock Copolymer Aligned Perpendicular to the Sample Plane—Transmission Electron-Microscopy and Small-Angle X-ray-Scattering. *Macromolecules* **1993**, *26*, 4373–4375.
23. Polis, D. L.; Smith, S. D.; Terrill, N. J.; Ryan, A. J.; Morse, D. C.; Winey, K. I. Shear-Induced Lamellar Rotation Observed in a Diblock Copolymer by *in Situ* Small-Angle X-ray Scattering. *Macromolecules* **1999**, *32*, 4668–4676.
24. Böker, A.; Elbs, H.; Hänsel, H.; Knoll, A.; Ludwigs, S.; Zettl, H.; Urban, V.; Abetz, V.; Müller, A. H. E.; Krausch, G. Microscopic Mechanisms of Electric-Field-Induced Alignment of Block Copolymer Microdomains. *Phys. Rev. Lett.* **2002**, *89*, 135502–5.
25. Böker, A.; Elbs, H.; Hänsel, H.; Knoll, A.; Ludwigs, S.; Zettl, H.; Zvelindovsky, A. V.; Sevink, G. J. A.; Urban, V.; Abetz, V.; *et al.* Electric Field Induced Alignment of Concentrated Block Copolymer Solutions. *Macromolecules* **2003**, *36*, 8078–8087.
26. Schmidt, K.; Böker, A.; Zettl, H.; Schubert, F.; Hänsel, H.; Fischer, F.; Weiss, T. M.; Abetz, V.; Zvelindovsky, A. V.; Sevink, G. J. A.; Krausch, G. Influence of Initial Order on the Microscopic Mechanism of Electric Field Induced Alignment of Block Copolymer Microdomains. *Langmuir* **2005**, *21*, 11974–11980.
27. Olszowka, V.; Kuntermann, V.; Böker, A. Control of Orientational Order in Block Copolymer Thin Films by Electric Fields: A Combinatorial Approach. *Macromolecules* **2008**, *41*, 5515–5518.
28. Olszowka, V.; Tsarkova, L.; Böker, A. 3-Dimensional Control over Lamella Orientation and Order in Thick Block Copolymer Films. *Soft Matter* **2009**, *5*, 812–819.
29. Böker, A.; Schmidt, K.; Knoll, A.; Zettl, H.; Hansel, H.; Urban, V.; Abetz, V.; Krausch, G. The Influence of Incompatibility and Dielectric Contrast on the Electric Field-Induced Orientation of Lamellar Block Copolymers. *Polymer* **2006**, *47*, 849–857.
30. Hund, M.; Herold, H. Design of a Scanning Probe Microscope with Advanced Sample Treatment Capabilities: An Atomic Force Microscope Combined with a Miniaturized Inductively Coupled Plasma Source. *Rev. Sci. Instrum.* **2007**, *78*, 063703.
31. Tsarkova, L.; Knoll, A.; Magerle, R. Rapid Transitions between Defect Configurations in a Block Copolymer Melt. *Nano Lett.* **2006**, *6*, 1574–1577.
32. Horvat, A.; Sevink, G. J. A.; Zvelindovsky, A. V.; Krekhov, A.; Tsarkova, L. Specific Features of Ddefect Structure and Dynamics in Cylinder Phase of Block Copolymers. *ACS Nano* **2008**, *2*, 1143–1152.
33. Constantin, D.; Oswald, P. Diffusion Coefficients in a Lamellar Lyotropic Phase: Evidence for Defects Connecting the Surfactant Structure. *Phys. Rev. Lett.* **2000**, *85*, 4297–4300.
34. Hubbard, P. L.; McGrath, K. M.; Callaghan, P. T. A Study of Anisotropic Water Self-Diffusion and Defects in the Lamellar Mesophase. *Langmuir* **2005**, *21*, 4340–4346.
35. Trebin, H. R. The Topology of Nonuniform Media in Condensed Matter Physics. *Adv. Phys.* **1982**, *31*, 195–254.
36. Mermin, N. D. Topological Theory of Defects in Ordered Media. *Rev. Mod. Phys.* **1979**, *51*, 591–648.
37. Pinna, M.; Schreier, L.; Zvelindovsky, A. V. Mechanism of Electric-Field-Induced Alignment of Block Copolymer Lamellae. *Soft Matter* **2009**, *5*, 970–973.
38. Hahm, J.; Lopes, W. A.; Jaeger, H. M.; Sibener, S. J. Defect Evolution in Ultrathin Films of Polystyrene-Block-Polymethylmethacrylate Diblock Copolymers Observed by Atomic Force Microscopy. *J. Chem. Phys.* **1998**, *109*, 10111–10114.
39. Hahm, J.; Sibener, S. J. Time-Resolved Atomic Force Microscopy Imaging Studies of Asymmetric Ps-B-Pmma Ultrathin Films: Dislocation and Disclination Transformations, Defect Mobility, and Evolution of Nanoscale Morphology. *J. Chem. Phys.* **2001**, *114*, 4730–4740.
40. Zvelindovsky, A. V.; Sevink, G. J. A. Microscopic Mechanisms of Electric-Field-Induced Alignment of Block Copolymer Microdomains. Comment. *Phys. Rev. Lett.* **2003**, *90*, 049601−049604.
41. Böker, A.; Abetz, V.; Krausch, G. Microscopic Mechanisms of Electric-Field-Induced Alignment of Block Copolymer Microdomains. Reply. *Phys. Rev. Lett.* **2003**, *90*, 049602−049605.
42. Choi, M. C.; Pfohl, T.; Wen, Z. Y.; Li, Y. L.; Kim, M. W.; Israelachvili, J. N.; Safinya, C. R. Ordered Patterns of Liquid Crystal Toroidal Defects by Microchannel Confinement. *Proc. Natl. Acad. Sci. U.S.A.* **2004**, *101*, 17340–17344.
43. Tsarkova, L.; Horvat, A.; Krausch, G.; Zvelindovsky, A. V.; Sevink, G. J. A.; Magerle, R. Defect Evolution in Block Copolymer Thin Films *via* Temporal Phase Transitions. *Langmuir* **2006**, *22*, 8089–8095.
44. Böker, A.; Müller, A. H. E.; Krausch, G. Nanoscopic Surface Patterns from Functional ABC Triblock Copolymers. *Macromolecules* **2001**, *34*, 7477–7488.
45. Hund, M.; Herold, H. German Patent No. 10 2004 043 191 B4 (24 May 2006) and U.S. Patent Application No. US 20080229812 A1 (25 Sep 2008).
46. Scherdel, S.; Wirtz, S.; Rehse, N.; Magerle, R. Non-Linear Registration of Scanning Probe Microscopy Images. *Nanotechnology* **2006**, *17*, 881–887.